

Magnetic structure of domain walls in stressed cylindrical wires

Ksenia A. Chichay, Igor S. Lobanov, Valery M. Uzdin

¹Department of Physics, ITMO University, St. Petersburg, 197101, Russia

^aks.chichay@gmail.com, ^blobanov.igor@gmail.com, ^cv.uzdin@mail.ru

Corresponding author: K. A. Chichay, ks.chichay@gmail.com

PACS 75.60.Ch, 75.30.Gw

ABSTRACT We investigate the internal structure and dynamics of transverse domain walls in amorphous, stressed ferromagnetic microwires by comparing two magnetoelastic anisotropy models. In the complete model, all three principal stress components (axial, radial, circumferential) extracted from a realistic stress profile are converted into spatially varying anisotropies; in the reduced model, only the dominant stress component in each radial region is retained. Micromagnetic simulations reveal that the reduced model produces exaggerated peripheral deviations—stronger radial magnetization projections and deeper penetration of the disturbed layer—compared to the complete model. Energy analysis shows that omitting non-dominant anisotropy leads to underestimation of domain wall-defect interactions and a sharp, shell-like radial ordering at higher values of surface anisotropy. Furthermore, dissipation calculations based on the Thiele approach indicate that the reduced model overestimates domain wall velocity by up to 50%. These results demonstrate that incorporating the full stress tensor is essential for accurate prediction of both static domain wall profiles and their dynamic response in stressed microwires.

KEYWORDS Domain wall, cylindrical wire, amorphous ferromagnetic microwires, micromagnetics, magnetoelastic anisotropy, internal mechanical stress.

ACKNOWLEDGEMENTS This work was funded by the Russian Science Foundation (project No. 23-72-10028, <https://rscf.ru/en/project/23-72-10028/>). K.A.Ch. acknowledges the support of ITMO Fellowship Program.

FOR CITATION Chichay K.A., Lobanov I.S., Uzdin V.M. Magnetic structure of domain walls in stressed cylindrical wires. *Nanosystems: Phys. Chem. Math.*, 2025, **16** (3), 325–332.

1. Introduction

The use of magnetoelastic interactions controlled by mechanical deformations in solids for the development of new information, sensor, and energy-saving technologies has led to the creation of a new direction in micro and nanoelectronics, called straintronics [1, 2]. Mechanical stresses can be associated with the magnetic or ferroelectric material, which manifests itself both in dynamic and static properties, and allows manipulation of the magnetic state and change in magnetic characteristics [3].

One such class of systems is the the amorphous ferromagnetic glass-coated microwires, which are a composite object with cylindrical symmetry consisting of a metallic nucleus and a glass shell [4, 5]. The peculiarity of such a microwire is the amorphous and stressed state of its metallic nucleus, due to its production using the Ulitovsky-Taylor method [6], which includes melt drawing and rapid quenching. Several types of stress coexist in an amorphous ferromagnetic microwire: i) stresses arising during rapid cooling, ii) stresses arising during the drawing process, and iii) stresses arising due to the difference in the thermal expansion coefficients of the metal and glass [7, 8].

Such coexistence of stresses leads to a certain, rather complex distribution of the three components of the mechanical stress tensor along the radius of the metal nucleus: axial (σ_{zz}), radial ($\sigma_{\rho\rho}$) and circumferential ($\sigma_{\phi\phi}$). The magnitude of internal mechanical stresses ranges from fractions to several units of gigapascals. Currently, there are several theoretical works that predict this distribution. In particular, the distribution of all three components of the mechanical stress tensor along the radius of the microwire, taking into account the solidification process, was calculated in [9].

Mechanical stresses together with the magnetostriction [10] effect determine the magnitude of magnetoelastic energy and, due to the amorphous state of the metallic nucleus along with the cylindrical shape, play a major role in the formation of the magnetic state and magnetic characteristics of the wire [9, 11–14]. In works published in the early 2000s, the authors considered the formation of magnetic anisotropy, directly dependent on the distribution of internal mechanical stresses along the radius of the metallic nucleus of the microwire [13]. Calculations were carried out for a microwire of composition $\text{Fe}_{77.5}\text{Si}_{7.5}\text{B}_{15}$ with a positive magnetostriction coefficient, a metallic nucleus diameter of 25 μm and a glass thickness of 15 μm . The authors determine the type and value of anisotropy in each part of the wire by taking into account the dominant component of mechanical stress.

In the distribution of stresses along the radius of the microwire, two regions can be distinguished: the region where the axial component has the largest value and is positive (tensile stress), and the region in which the circumferential and axial components of stress are negative (compressive stress) and have the greatest absolute value [9, 13]. We will call these two areas conditionally the center and the periphery. If we take into account only the dominant component of mechanical stresses, then the determination of the anisotropy type occurs in the following way. In the case of positive magnetostriction, axial tensile stresses in the center will then induce an easy-axis axial anisotropy, which will prevail in almost the entire volume of the metallic nucleus of the wire with the average value of $K^{\text{rad}} = 3 \cdot 10^4 \text{ J/m}^3$. At the peripheral layer, where negative circumferential stresses are dominant in magnitude, the resulting easy-axis anisotropy must be perpendicular to this direction, so it will be either axial or radial. But since in this region the axial compressive stresses are also large, the resulting direction of easy-axis anisotropy satisfying both types of stresses will be radial with the maximum value of $K^{\text{rad}} = 5.6 \cdot 10^4 \text{ J/m}^3$ (the value corresponds to circumferential mechanical stresses at the periphery). It is this distribution of anisotropy that is usually taken into account when discussing the formation of the domain structure of microwires and domain wall configuration.

In this work, we consider how taking into account all three types of stress affects the structure of transverse domain wall. We refer to such consideration as the complete model and compare it with the results obtained for the reduced model (when only the dominant component is taken). We discuss the change in the domain wall internal structure with a change in the anisotropy value at the periphery and analyze the energy contributions for the both cases of complete and reduced models.

2. Model

We simulate magnetic domain walls (DWs) in a cylindrical wire using a custom-developed Magnes software. The system under study is a wire with fixed geometry: length L and radius R . Equilibrium DW configurations are obtained by minimizing the micromagnetic energy functional, containing contributions of symmetric exchange E^{ex} and three anisotropies: axial E^{ax} , radial E^{rad} , and circumferential E^{circ} :

$$E = E^{\text{ex}} + E^{\text{ax}} + E^{\text{rad}} + E^{\text{circ}}. \quad (1)$$

The first term in (1) corresponds to the exchange energy, with exchange stiffness $A = 2 \cdot 10^{-11} \text{ J/m}$

$$E^{\text{ex}} = \frac{A}{2} \iiint \left[\left(\frac{\partial \mathbf{S}}{\partial \rho} \right)^2 + \frac{1}{\rho^2} \left(\frac{\partial \mathbf{S}}{\partial \phi} \right)^2 + \left(\frac{\partial \mathbf{S}}{\partial z} \right)^2 \right] dV,$$

where $\mathbf{S}(\rho, \phi, z)$ is the magnetization vector field. The z-axis is aligned with the wire axis, while ρ and ϕ are polar coordinates in the cross-sectional plane. Three anisotropy contributions are defined by corresponding spatially varying parameters $K^i(\rho)$ and axis \mathbf{e}^i , where \mathbf{e}^z is unit vector along z-axis, $\mathbf{e}^{\text{rad}} = \mathbf{e}^\rho$ and $\mathbf{e}^{\text{circ}} = \mathbf{e}^\phi$ are local orthonormal basis in polar coordinates in the wire cross section:

$$E^i = - \iiint K^i(\rho) (\mathbf{S} \cdot \mathbf{e}^i)^2 dV, \quad i = \text{ax, rad, circ}.$$

The energy density corresponding to energy contribution E^i is denoted w^i . In our simulations, we consider a wire of radius $R = 10^{-7} \text{ m}$ and length $L = 10^{-6} \text{ m}$.

The micromagnetic problem was discretized on a cylindrical grid with the following resolution: $N_\rho = 15$ points in the radial direction (from the wire center to the boundary), $N_\phi = 40$ angular divisions, and $N_z = 200$ points along the wire axis. The energy functional was approximated using central finite differences for spatial derivatives and the trapezoidal rule for numerical integration. This discretization scheme yields a second-order accuracy, with an error scaling as $O(h^2)$ for the exchange energy, where h denotes the grid spacing [15].

The non-zero anisotropy contributions and the spatial distribution of the magnetoelastic anisotropy $K_i(\rho)$ were defined differently in the two modeling approaches mentioned above. In both cases, the magnetoelastic anisotropy arises from internal mechanical stresses and is given by

$$K_{\text{me}}^i = \frac{3}{2} \lambda_S \sigma_{ii}, \quad i = \text{ax, rad, circ},$$

where λ_S is saturation magnetostriction coefficient and σ_{ii} is the diagonal stress component. In both models, we also account for the effective shape anisotropy of the cylinder, arising from the demagnetizing field. This contribution is included as an additional uniaxial anisotropy term with strength $K_{\text{eff}}^{\text{ax}} = 1/4 \mu_0 M_s^2$ where $M_s = 500 \text{ kA/m}$ is the saturation magnetization. Radial and circumferential anisotropy contain only the magnetoelastic anisotropy:

$$K^{\text{ax}} = K_{\text{me}}^{\text{ax}} + K_{\text{eff}}^{\text{ax}}, \quad K^{\text{circ}} = K_{\text{me}}^{\text{circ}}, \quad K^{\text{rad}} = K_{\text{me}}^{\text{rad}}.$$

In the first approach, referred to as the *reduced model*, only a single dominant magnetoelastic anisotropy component was assigned to each region of the wire, reflecting the prevailing stress orientation and magnitude. Specifically, in the wire core, an easy-axis axial anisotropy was imposed, with a average value of $K_{\text{me}}^{\text{ax}} = 3 \cdot 10^4 \text{ J/m}^3$. At the periphery, an

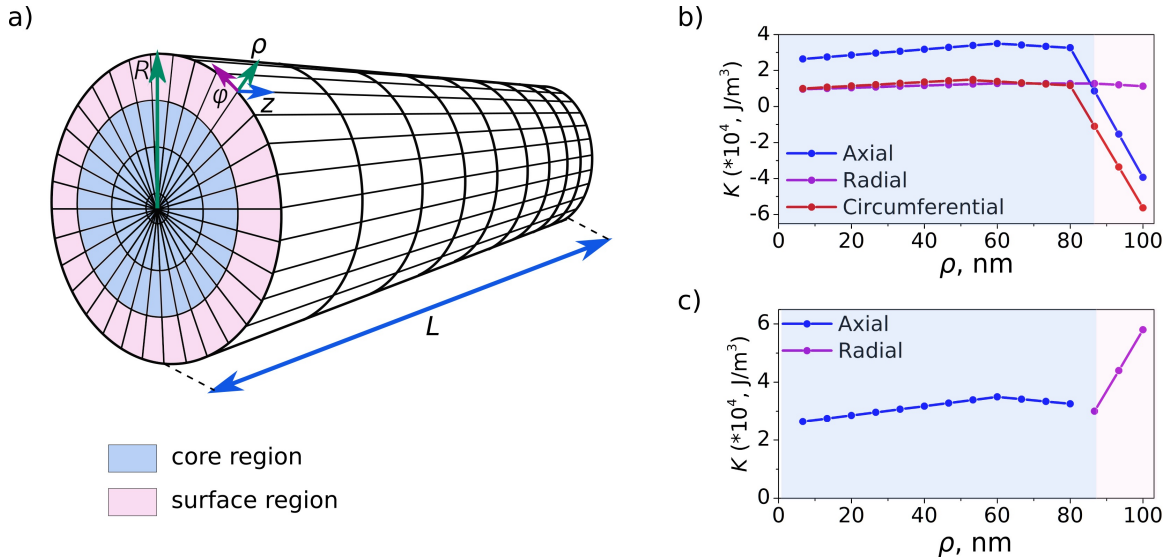


FIG. 1. a) Schematic representation of a wire in cylindrical coordinate system. R is the wire radius, L is the length of the wire. b) and c) Radial dependence of magnetoelastic anisotropy components in the complete and reduced models, respectively. Light blue and light pink areas correspond to the core and surface regions

easy-axis radial anisotropy was applied, reaching up to $K_{\max}^{\text{rad}} = 5.6 \cdot 10^4 \text{ J/m}^3$ at the surface layer. Further details can be found in the previously cited work [13]. Radial profiles of magnetoelastic anisotropies are shown in Fig. 1c.

The second approach, referred to as the *complete model*, incorporates all three components of internal stress (axial, radial, and circumferential) each distributed along the wire radius (Fig. 1b). Following the methodology of [13], tensile stresses are translated into easy-axis anisotropy, while compressive stresses correspond to easy-plane anisotropy. As a result, all three types of anisotropy are present throughout the entire wire volume, with their radial distributions directly reflecting the magnitude and sign of the underlying stresses. The stress profile was adopted from [13], and the magnetostriction coefficient was set to $\lambda_S = 25 \cdot 10^{-6}$, a typical value for Fe-based microwires. The maximum anisotropy values at the wire surface were $K_{\max}^{\text{circ}} = -5.6 \cdot 10^4 \text{ J/m}^3$ for the circumferential component and $K_{\max}^{\text{ax}} = -3.9 \cdot 10^4 \text{ J/m}^3$ for the axial component. The radial profiles of the anisotropy components reveal two distinct regions: a *core region* $\rho < 87 \text{ nm}$, and a *surface region* $\rho > 87 \text{ nm}$, which are shown in Fig. 1a. In the core, all three anisotropies remain virtually constant, but the axial anisotropy dominates in magnitude. In contrast, in the surface layer both the axial and circumferential anisotropy components vary more strongly with ρ , and notably, change sign as one moves to the surface, while radial anisotropy maintains its value practically constant. This sign reversal reflects the shift from tensile to compressive stress regimes across the wire radius.

To investigate the influence of peripheral anisotropy $K^i(R)$ we kept the anisotropy constants fixed in the inner region of the wire and modified them only within the surface region. To ensure smooth spatial variation, a linear interpolation was applied between the anisotropy values in the inner region and those at the surface. The maximum absolute anisotropy value was always attained at the surface. Surface anisotropy was controlled by a scaling factor k such that $K^i(R) = kK_{\max}^i$, where K_{\max}^i denotes the maximum anisotropy strength. The same scaling factor was applied to both the radial easy-axis magnetoelastic anisotropy component in reduced model and easy-plane axial and circumferential components of magnetoelastic anisotropy in the complete model.

3. Domain wall structure

We consider a metastable state of a cylindrical microwire, comprising two oppositely magnetized domains separated by a transverse head-to-head domain wall. As demonstrated in our previous work [16], radially inhomogeneous anisotropy can lead to deviations from the conventional internal structure of the domain wall. In the present case, these deviations emerge near the wire periphery, where the strong anisotropy favors directions other than the axial easy axis. In contrast, near the wire center (where the axial easy-axis anisotropy dominates) the magnetization remains predominantly transverse. Under these conditions, the transverse domain wall can be viewed as consisting of two sectors (typically symmetric), each characterized by a magnetization component with a radial projection. In one sector, the magnetization points inward toward the wire center; in the other, outward. Both sectors are aligned with the preferred transverse direction at the wire core. This configuration represents a compromise between a conventional transverse domain wall and one where the magnetization is entirely radial. A domain wall with such an internal structure is illustrated in Fig. 2.

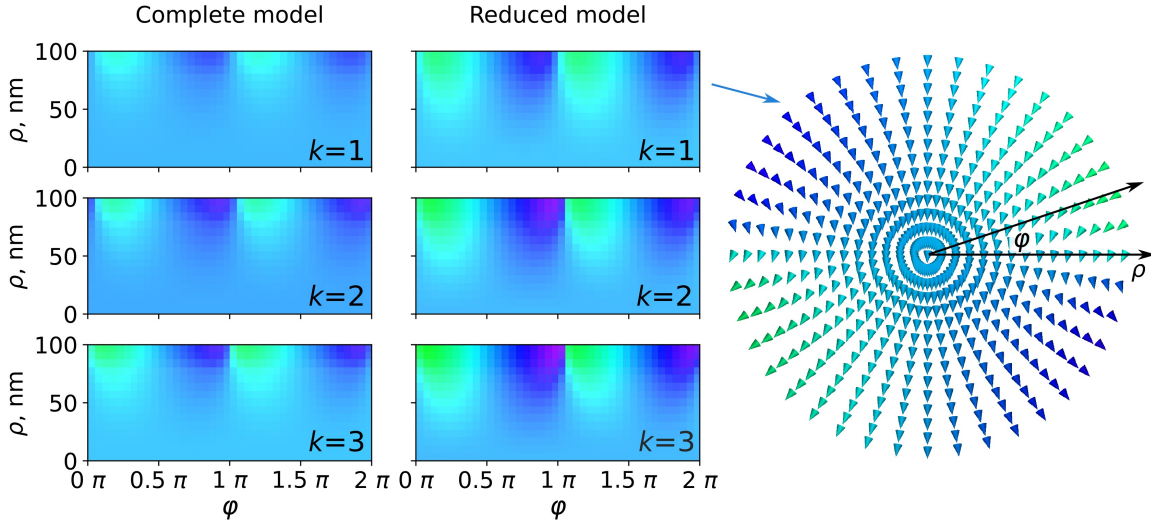


FIG. 2. Evolution of the magnetic configuration of the transverse DW with a change of the anisotropy value at the periphery for the cases of complete and reduced models. For each anisotropy value k , an unrolled view of the $\rho - \phi$ DW cross section is given.

To provide a more intuitive visualization, we present domain wall structures using an unrolled $\rho - \phi$ view instead of a circumferential cross-section. Fig. 2 illustrates domain wall configurations at the wire periphery for different values of the scaling factor k , comparing the complete and reduced anisotropy models. The top row in each column corresponds to $k = 1$, with parameters taken from [13]. In both models, the same general type of domain wall is stabilized; however, the extent of peripheral magnetization deviation differs significantly. In the reduced model, deviations from the ideal transverse wall are much more pronounced. Specifically, magnetic moments near the surface exhibit larger angular deviations from the transverse direction imposed by the wire center. Additionally, the perturbation penetrates deeper into the wire compared to the complete model. As the peripheral anisotropy strength increases (i.e., as k increases), the models exhibit more pronounced deviations, characterized by stronger radial projections of the magnetization and deeper penetration into the wire core. Nevertheless, even at $k = 3$, the complete model shows smaller deviations than the reduced model at $k = 1$. This highlights the stabilizing effect of including all three anisotropy components in the complete model, which helps preserve the transverse domain wall structure across a broad range of peripheral anisotropy values.

To gain deeper insight into the domain wall structure, we analyze the contributions of each anisotropy component separately. Fig. 3a presents the spatial distribution of the axial anisotropy energy density, w^{ax} across the domain wall cross-section for various values of the peripheral anisotropy scaling factor k . Each cross-section reveals two distinct regions: a central zone (in blue) and a peripheral zone (in green), separated by a narrow transition region characterized by a minimum in anisotropy energy density (dark blue). Importantly, the magnitude and spatial uniformity of w^{ax} in the wire center remain unchanged with increasing k , reflecting the fact that the axial anisotropy constant is held fixed in this region. In contrast, the peripheral value of w^{ax} increases proportionally with k . Notably, the thickness of the outer shell where w^{ax} approaches zero behaves differently in the two models: it remains constant in the complete model, whereas in the reduced model it increases with k . This indicates a more pronounced sensitivity of the reduced model to peripheral anisotropy modulation.

Figure 3b shows how the total axial anisotropy energy, E^{ax} , varies with the peripheral anisotropy scaling factor k . The energy is computed relative to that of a uniformly magnetized (homogeneous ferromagnetic) reference state. The plot reveals that E^{ax} at the wire center is identical for both the complete and reduced models only at $k = 1$. As k varies, the two models exhibit opposite trends: in the complete model, E^{ax} increases slightly, while in the reduced model it decreases. This energy dependence highlights a key feature of the micromagnetic structure obtained in the reduced model. Beyond a certain threshold value $k > X$, the domain wall at the wire surface becomes significantly wider. In this regime, the radial orientation of the magnetic moments at the periphery begins to spread symmetrically outward from the domain wall, forming a radially ordered “shell”. The sharp drop in E^{ax} observed for the reduced model starting at $k = 2$ corresponds to the formation of this shell throughout the wire volume.

Figure 3c shows the spatial distribution of the radial anisotropy energy density, w^{rad} , across the domain wall cross-section. In the reduced model, radial anisotropy is applied only in the peripheral layer of the wire, resulting in $w^{\text{rad}} = 0$ in the central region. In contrast, the complete model assigns radial anisotropy throughout the entire wire volume, though its magnitude remains constant with respect to k . Consequently, the spatial pattern of w^{rad} remains largely unchanged across different values of k in the complete model. The minima of w^{rad} (indicated by dark blue regions) correspond to areas where the magnetization aligns closely with the radial direction. As k increases, the radial projection of the magnetization

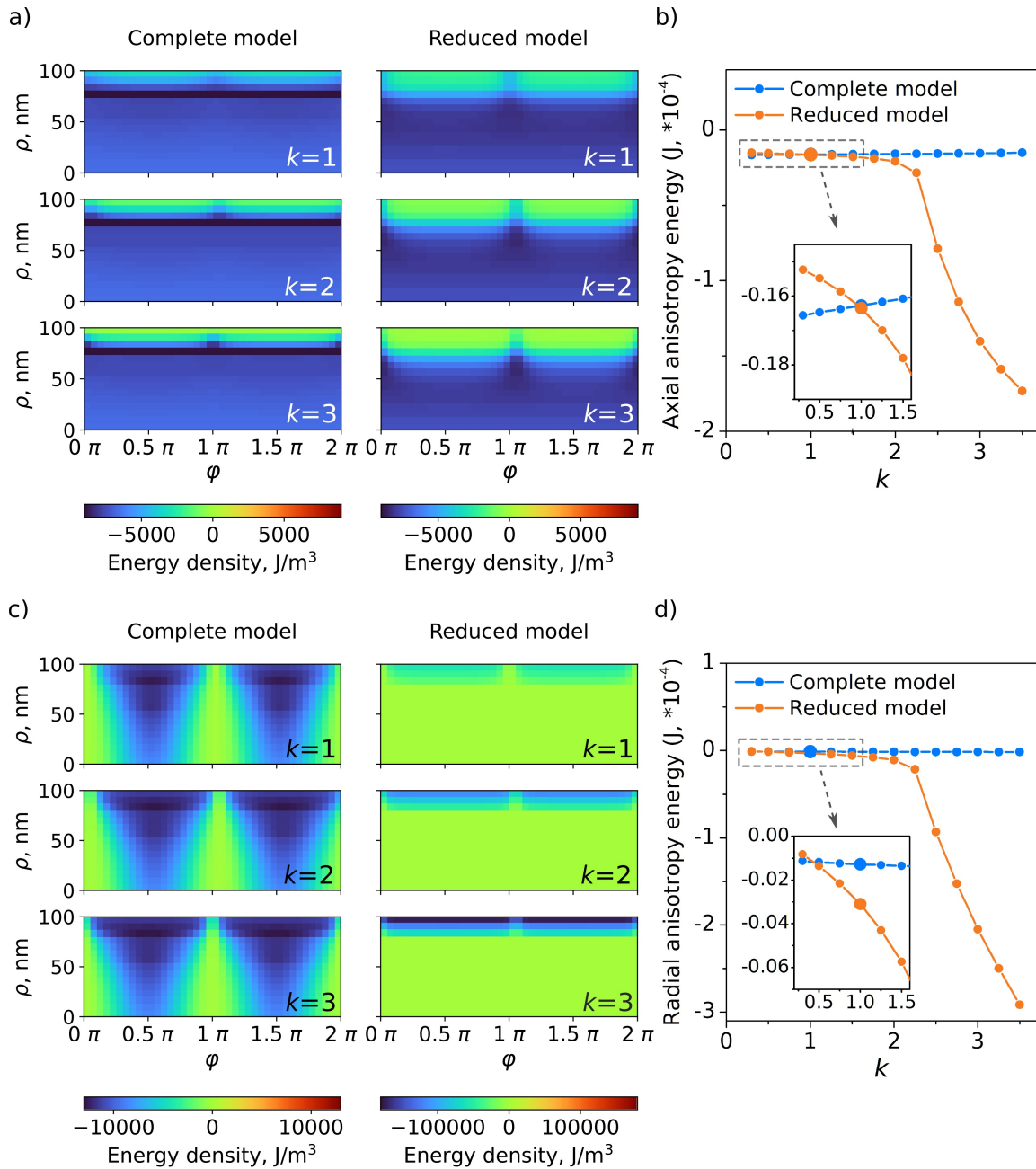


FIG. 3. (a) and (c) Distributions of axial and radial anisotropy energy density for an unrolled $\rho - \phi$ DW cross section for different values of k . The color bar indicates the energy density value from the lowest negative (dark blue) to the highest positive (dark red) value. (b) and (d) Axial and radial anisotropy energy as a function of anisotropy value at the periphery k for the cases of complete and reduced models. The largest dots on the graph are related to the $k = 1$.

grows in both halves of the wall, causing the low-energy regions near the surface to expand slightly. The corresponding dependence of the total radial anisotropy energy, E^{rad} on the scaling factor k is presented in Fig. 3d. The two models agree only at small values of k . For the reduced model, a sharp drop in E^{rad} occurs as k increases, which reflects the emergence of a fully formed radially ordered layer that extends along the wire surface. This pronounced difference in w^{rad} between the complete and reduced models is expected to significantly influence both the structure and dynamic behavior of moving domain walls, including their shape and velocity.

Figure 4a presents the distribution of circumferential anisotropy energy density, w^{circ} , for the complete model only, as circumferential anisotropy is not included in the reduced model. In the domain wall cross-sections, nonzero values of w^{circ} are observed exclusively in “transitional” regions—specifically, at the boundary between two sectors where the magnetization points radially inward in one and outward in the other. Notably, circumferential anisotropy is the only anisotropy component for which the energy density assumes both positive and negative values. The extrema of w^{circ}

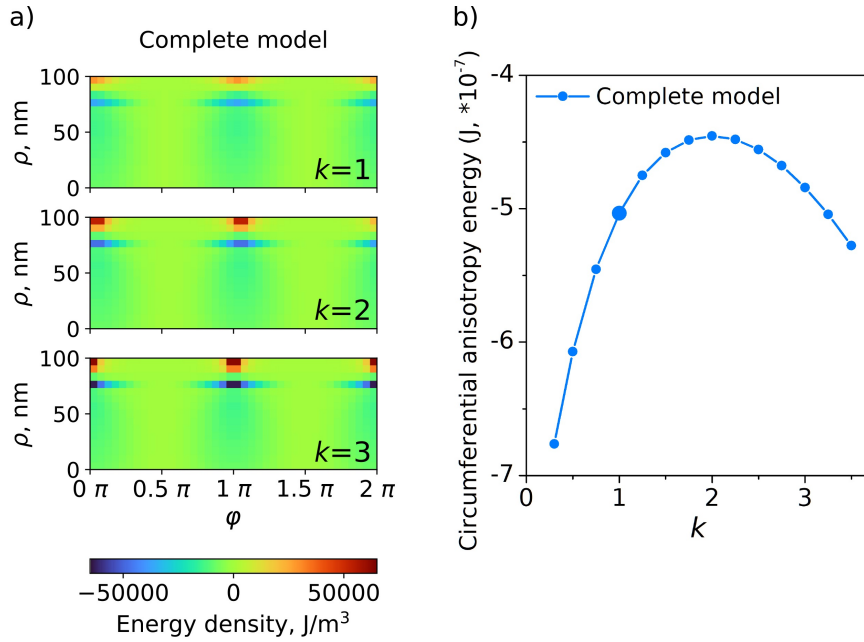


FIG. 4. Distribution of circumferential anisotropy energy density for an unrolled ρ – ϕ DW cross section for different values of k . (b) Circumferential anisotropy energy as a function of anisotropy value at the periphery k for the case of complete model. The largest dot on the graph is related to the $k = 1$.

are highly localized in both angular and radial coordinates. This spatial confinement may play an important role in domain wall interactions with defects and impurities. Such interactions can be considered from two perspectives. First, because the maxima and minima of w^{circ} are sharply localized and occur at specific depths, the nature of the domain wall's interaction with a given impurity—whether attractive or repulsive—depends critically on the impurity's radial position. Second, domain walls in cylindrical wires exhibit azimuthal rotation during motion due to the cylindrical symmetry (i.e., energetic equivalence of all transverse directions). As a result, interaction with an impurity also depends on whether the rotating anisotropy features (such as the localized maxima/minima of w^{circ}) spatially overlap with the impurity, and on the impurity's size. This interplay can have a significant impact on domain wall dynamics, particularly affecting the domain wall velocity and the nucleation field (i.e., the critical magnetic field required to nucleate a domain wall inside the microwire). Since circumferential anisotropy is omitted in the reduced model, it may underestimate the strength and complexity of domain wall-defect interactions.

The behavior of the total circumferential anisotropy energy, E^{circ} shown in Fig. 4b, exhibits a non-monotonic trend: it increases with the scaling factor k up to $k = 2$, and then begins to decrease. This trend likely arises from the interplay between the localized minima and maxima of the energy density w^{circ} , which evolve with increasing k . As k increases, the radial extent of magnetization deviations at the wire periphery also increases. Consequently, the region at the boundary between the two radially magnetized sectors of the domain wall—where the magnetization momentarily aligns in the circumferential direction—expands. This expansion can lead to a faster growth in the magnitude of the negative (minimum) values of w^{circ} , which may dominate the total energy and result in the observed decrease in E^{circ} beyond a certain k .

Figure 5a shows the total energy of the wire as a function of the scaling factor k , revealing opposite trends for the complete and reduced models: the system energy slightly grows in the complete model and decreases in reduced model. Note, that the energy is computed relative to that of a uniformly magnetized (homogeneous ferromagnetic) reference state. For small k the energies of obtained magnetic states are almost coincides. As the anisotropy in the surface layer k increases, the differences in energies become noticeable. Hence, it can be assumed that for large anisotropies at the periphery the applicability of the reduced model is questionable.

4. Domain wall movement

Domain walls (DWs) in magnetic wires are typically driven by external magnetic fields. In the simplest scenario, a uniform field H is applied along the axis of the wire. One domain, aligned with the field, is energetically favored, while the oppositely oriented domain becomes unfavorable. As the system relaxes, the domain aligned with the field expands, and the opposing domain shrinks.

The dynamics of such a system are governed by the Landau-Lifshitz-Gilbert (LLG) equation, which can lead to complex phenomena, including the formation, motion, and detachment of singularities in the magnetization texture. However, in this study, we provide a simplified estimate of the DW velocity by assuming the domain wall maintains a fixed shape during motion.

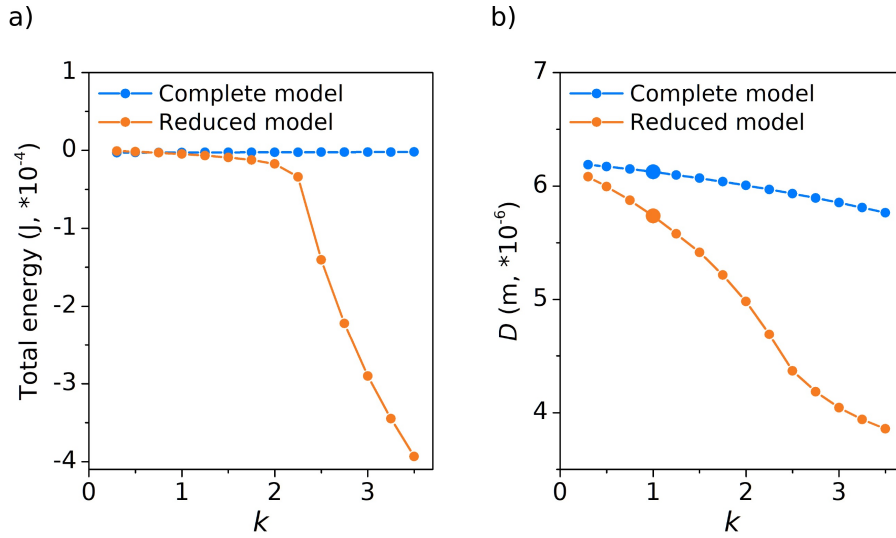


FIG. 5. (a) Total energy as a function of anisotropy value at the periphery k for the cases of complete and reduced models. (b) Value of the dissipation D as a function of anisotropy value at the periphery k .

Under the assumption that only the DW position changes while all internal degrees of freedom remain fixed, the LLG equation reduces to the Thiele equation [17]. Let the domain wall be described by a traveling ansatz of the form:

$$\mathbf{S}(\mathbf{r}, t) = \mathbf{S}_0(\mathbf{r} - R(t)\mathbf{e}^z),$$

where \mathbf{S}_0 is the static DW profile, R is the DW position at time t . Substituting this ansatz into the LLG equation and projecting onto the subspace spanned by $\partial\mathbf{S}/\partial R$, we obtain the Thiele equation in the general form [18]:

$$\alpha DV - GV = F,$$

where $V = \dot{R}$ is the DW velocity, α is the Gilbert damping parameter, D is the dissipation matrix, G is the gyrotropic tensor, and F is the net force (or generalized torque) acting on the wall. In our case, the DW position is described by a single parameter R , and the gyrotropic term G vanishes due to the antisymmetry of the gyrotropic tensor and the absence of azimuthal precession in the ansatz. The dissipation reduces to a scalar quantity given by:

$$D = \int_{\Omega} \left(\frac{\partial \mathbf{S}}{\partial z} \right)^2 dV,$$

which corresponds to the portion of the exchange energy associated with deformations along the wire axis. The driving force F is given by derivative of total energy E with respect to the DW position:

$$F = -\frac{\partial E}{\partial R} = 2M_s H s,$$

where s is the cross-sectional area of the wire. This result follows from translational symmetry: shifting the DW by dR effectively reverses the magnetization in a volume $s \cdot dR$, yielding a change in Zeeman energy proportional to H . Assuming the DW shape remains unchanged during motion, the force F becomes independent of position, and the DW velocity simplifies to:

$$V = \frac{F}{\alpha D} \sim \frac{1}{D}.$$

We computed the dissipation coefficient D for both the reduced (1-axis) and complete (3-axis) anisotropy models across a range of surface anisotropy strengths. The results are presented in Fig. 5b. Under the considered parameters, the domain wall in the complete model moves approximately 1.5 times slower than in the reduced model, due to higher dissipation. This implies that simulations based on the simplified reduced model are likely to overestimate DW velocity. The discrepancy becomes even more pronounced at higher anisotropy strengths.

5. Conclusion

We studied the structure of transverse domain walls (DWs) in amorphous, stress-induced magnetic wires using two models of magnetoelastic anisotropy: the complete model, which accounts for all stress components throughout the wire volume, and the reduced model, which includes only the dominant stress component, converted into anisotropy. While both models yield domain walls of the same general type, their internal structures differ significantly.

In the reduced model, deviations of the magnetization near the wire surface are more pronounced, and these disturbances penetrate deeper into the wire compared to the complete model. An analysis of how the DW structure evolves with

increasing anisotropy at the periphery reveals that the complete model better preserves the transverse character of the DW over a wider range of anisotropy strengths.

Notably, the omission of circumferential anisotropy in the reduced model may lead to an underestimation of the domain wall's interaction with defects and impurities. At the same time, it tends to overestimate the DW velocity, due to lower calculated dissipation in the system.

References

- [1] Bukharaev A.A., Zvezdin A.K., Pyatakov A.P., Fetisov Y.K. Straintronics: a new trend in micro- and nanoelectronics and materials science. *Physics-Uspokhi*, 2018, **61**(12), P. 1175.
- [2] Bandyopadhyay S., Atulasimha J., and Barman A. Straintronics: Manipulating the Magnetization of Magnetostrictive Nanomagnets with Strain for Energy-Efficient Applications. *Applied Physics Reviews*, 2021, **8**, P. 041323.
- [3] Pyatakov A., Zvezdin A. Magnetolectric and multiferroic media. *Physics-Uspokhi*, 2012, **55**(6), P. 557–581.
- [4] Alam J., et.al. Cylindrical micro and nanowires: Fabrication, properties and applications. *J. Magn. Magn. Mater.*, 2020, **513**, P. 167074.
- [5] Chiriac H., Corodeanu S., Lostun M., Stoian G., Ababei G., and Óvári T.A. Rapidly solidified amorphous nanowires. *J. Appl. Phys.*, 2011. **109**(6), P. 063902.
- [6] Baranov S.A., Larin V.S., Torcunov A.V., Technology, Preparation and Properties of the Cast Glass-Coated Magnetic Microwires. *Crystals*, 2017. **7**(136).
- [7] Chiriac H., Ovari T.A. and Pop Gh. Internal stress distribution in glass-covered amorphous magnetic wires. *Phys. Rev. B*, 1995, **42**, P. 10104.
- [8] Liu K., Lu Z., Liu T., Li D. Measurement of internal tensile stress in $\text{Co}_{68.2}\text{Fe}_{4.3}\text{Cr}_{3.5}\text{Si}_{13}\text{B}_{11}$ glass-coated amorphous microwires using the stress sensitivity of saturation magnetostriction. *J. Magn. Magn. Mater.*, 2013. **339**, P. 124–126.
- [9] Chiriac H., Ovari T.-A., Switching field calculations in amorphous microwires with positive magnetostriction. *J. Magn. Magn. Mater.*, 2002, **249**, P. 141–145.
- [10] Churyukanova M., Semenkov V., Kaloshkin S., Shuvaeva E., Gudoshnikov S., Zhukova V., and Zhukov A., Magnetostriction investigation of soft magnetic microwires. *Phys. Stat. Sol. (a)*, 2016, **213**(2), P. 363–367.
- [11] Aksenova O.I., Orlova N., Churyukanova M.N., Aronin A.S. Stress state effect on the magnetic properties of amorphous microwires. *J. Magn. Magn. Mater.*, 2020, **495**, P. 165878.
- [12] Nematov M.G., Baraban I., Yudanov N.A., Rodionova V., Qin F.X., Peng H.-X., Panina L.V., Evolution of the magnetic anisotropy and magnetostriction in Cobased amorphous alloys microwires due to current annealing and stress-sensory applications. *J. Alloys. Compd.*, 2020, **837**, P. 155584.
- [13] Chiriac H., Ovari T.-A., Zhukov A. Magnetoelastic anisotropy of amorphous microwires. *J. Magn. Magn. Mater.*, 2003, **496**, P. 254–255.
- [14] Zhukova V., Blanco J.M., Ipatov M., Zhukov A. Magnetoelastic contribution in domain wall dynamics of amorphous microwires. *Physica B*, 2012, **407**, P. 1450–1454.
- [15] Chichay K.A., Lobanov I.S. Uzdin V.M. Stability and transformations of domain walls in cylindrical wires. *Nanosystems: Phys. Chem. Math.*, 2024, **15**(3), P. 332–339.
- [16] Chichay K.A., Lobanov I.S., Uzdin V.M. The structure of magnetic domain walls in cylindrical nano- and microwires with in- homogeneous anisotropy. *Nanosystems: Phys. Chem. Math.*, 2023, **15**(1), P. 55–59.
- [17] Thiele A.A. Steady-state motion of magnetic domains. *Phys. Rev. Lett.*, 1973, **30**, P. 230–233.
- [18] Lobanov I.S., Uzdin V.M. Dynamics of "Breathing" Skyrmions. *JETP Letters*, 2024, **119**(10), P. 768–774.

Submitted 6 April 2025; revised 6 May 2025; accepted 7 May 2025

Information about the authors:

Ksenia A. Chichay – Department of Physics, ITMO University, St. Petersburg, 197101, Russia; ORCID 0000-0002-6921-6075; ks.chichay@gmail.com

Igor S. Lobanov – Department of Physics, ITMO University, St. Petersburg, 197101, Russia; ORCID 0000-0001-8789-3267; lobanov.igor@gmail.com

Valery M. Uzdin – Department of Physics, ITMO University, St. Petersburg, 197101, Russia; ORCID 0000-0002-9505-0996; v.uzdin@mail.ru

Conflict of interest: the authors declare no conflict of interest.